TRENDS IN SCIENCES 2025; 22(9): 9839
https://doi.org/10.48048/tis.2025.9839 RESEARCH ARTICLE

Optimizing Starch Extraction from Porang Glucomannan Extraction Residue using Ultrasonic-Assisted Extraction: A Comparative Approach

Nurul Fadillah Arshy, Yudi Pranoto* and Manikharda

Department of Food and Agricultural Product Technology, Faculty of Agricultural Technology, Universitas Gadjah Mada, Yogyakarta 55281, Indonesia

(*Corresponding author's e-mail: pranoto@ugm.ac.id)

Received: 22 January 2025, Revised: 4 February 2025, Accepted: 11 February 2025, Published: 1 July 2025

Abstract

This study optimized starch extraction from porang glucomannan extraction residue (PR) using Response Surface Methodology (RSM) with a Box-Behnken design. Ultrasonic-Assisted Extraction (UAE) was employed, focusing on sonication power, extraction time, and solid-to-solvent ratio. A second-order polynomial model with high accuracy (R^2 = 0.9972) identified optimal conditions as 119.97 W sonication power, a 1:39.88 g/mL solid-to-solvent ratio, and 18.89 min extraction time. The experimental yield of 77.54 % surpassed the predicted value, confirming UAE's efficiency for industrial-scale extraction. Optimized porang starch (OPS) showed the highest starch (67.80 %) and amylose (24.73 %) content, while starch from residue (OPRS) had lower starch (55.69 %) and amylose (7.51 %) but higher amylopectin (48.18 %). Color analysis revealed lighter, whiter starches, indicating effective pigment removal. FTIR confirmed the structural integrity and purity of both OPS and OPRS, while XRD showed comparable crystallinity, with a slight increase in OPRS. Microscopic analysis revealed uniform, smoother granules in OPS. DSC analysis indicated higher thermal stability and gelatinization temperatures in OPS compared to porang starch (PS) and porang flour (PF). These findings highlight UAE as an effective method for extracting high-quality starch from porang residue, with potential applications in industries, supporting sustainable practices and efficient resource utilization.

Keywords: Amylose, Sonication power, Solid-solvent ratio, Starch characterization, Extraction optimization, UAE, Porang residue, RSM, Sustainable practices

Introduction

Porang (*Amorphophallus muelleri* Blume) is a plant that thrives in tropical regions, particularly in Indonesia. It is commonly processed into porang flour, which contains a starch content of approximately 63.30 % [1]. Another study reported that 1 kg of porang tubers produces 152 g or 15.2 % starch [2]. In addition to starch, porang is rich in glucomannan, comprising 40 - 90 % of its composition. This compound possesses significant physiological properties, making it highly valuable as a raw material in the food industry [3-6]. Economically, porang plays an essential role across various industries, including food, pharmaceuticals, and cosmetics [2,7-11]

The glucomannan extraction process from porang tubers generates a substantial amount of residue. According to Nasrullah *et al*. [12] reported that glucomannan derived from agro-industrial waste contains 49.42 % carbohydrates, with 34.62 % being starch. While this starch can be converted into liquid sugar, the low yield achieved through existing extraction methods highlights the need for further optimization. Ultrasonic-assisted extraction (UAE) has been identified as a promising technique for starch extraction, as it enhances solvent penetration into plant tissues, thereby accelerating the extraction and isolation process. Research indicates that variations in sonication power and duration have a notable impact on the properties of the extracted starch. UAE is widely regarded as a fast, efficient, and eco-friendly method that preserves the quality of starch isolates [13-18].

Related studies have also explored the isolation of starch from residues of purple yam anthocyanin extraction [19,20].

Response Surface Methodology (RSM) combined with UAE has been widely applied and shown to be highly effective in optimizing starch extraction from various sources, such as cassava tubers, maize starch, sago, sweet potatoes, and others [19-22]. It has also been utilized to enhance starch extraction from waste materials, including sago pith *Noor et al. [*21], and oil palm trunk [23]. Despite these advancements, no prior research has employed an RSM-based approach to optimize starch extraction from porang glucomannan extraction residue (PR). Previous studies have shown that starch residues can be used in bio-based materials such as biodegradable plastics, or as thickeners in food products due to their unique physicochemical properties. Exploring such applications not only adds value to waste but also supports sustainable development [24]. This study provides a foundation for identifying the key properties of porang starch residues that align with these applications.

Although previous studies have explored the extraction and characterization of porang products, they have not specifically focused on the starch derived from PR. This research addresses this gap by optimizing the starch extraction process, conducting comprehensive characterization, and comparing the properties of the extracted starch with those of porang flour (PF) and porang starch (PS). Such a comparison enables a deeper understanding of the distinct characteristics of the starch extracted from PR. This study utilizes RSM to optimize the starch extraction process from PR, a method renowned for fine-tuning extraction parameters across various starch sources [17,19-21,25,26]. The research investigates critical factors influencing the extraction process, including Ultrasonic-Assisted Extraction (UAE) power, extraction duration, and the solvent-to-sample ratio. Through this optimization, the study aims to maximize starch recovery with superior quality from glucomannan extraction residues. Ultimately, the findings of this study contribute to advancements in food technology, enhance the economic value of porang-based products, and expand the potential applications of starch in various industries.

Materials and methods

Materials

The main ingredient was PR obtained from KITAGAMA Laboratory, Universitas Gadjah Mada, Yogyakarta. The chemicals used include sodium metabisulfite (Merck KGaA, Germany), HCl (Smart-Lab, Indonesia), NaOH (Merck KGaA, Germany), acetic acid (Merck KGaA, Germany), iodine (Smart-Lab, Indonesia), ethanol 96 % (Merck KGaA, Germany), and distilled water.

Methods

Sample preparation

Porang glucomannan was extracted from PF, which was prepared by slicing the porang tubers into thin slices (± 3 mm), drying them at 60 °C, and then grinding them into flour. The extraction was performed by adding aluminum sulfate and sodium metabisulfite. The chemicals were dissolved in 5 L of water, followed by the addition of 100 g of porang flour. The resulting mixture was stirred in a water bath maintained at 75 °C. Afterward, the mixture was diluted with 5 L of water and filtered through a cloth to obtain filtrate. 96 % ethanol (ethanol = 1:1) was added to the filtrate to precipitate the glucomannan. The resulting precipitate (cloud) was filtered using a fine cloth. The glucomannan extraction residue was then dried at 55 °C for approximately 12 h. The dried sample was milled and passed through a 100-mesh sieve, while the residue was re-milled and sieved again [27]. The Glucomannan extraction residue was then subjected to further starch extraction. Fifty milliliters of the porang glucomannan extraction residue were centrifuged at 4,000 rpm for 15 min. The sediment separated from the supernatant was collected and dried in a cabinet dryer at 50 °C for 24 h [28].

Porang glucomannan extraction residue starch extraction

The pre-treated PR was transferred to a beaker, and a 0.2 % sodium metabisulfite solution was added. The mixture underwent with an ultrasonic probe (UP200St, 200W, 26 KHz, Hielscher, Germany). The starch suspension from the PR was subjected to different ultrasonic power levels and sonication times. The extraction temperature was controlled by circulating water through a double-jacketed beaker, with the

ultrasonic probe submerged 28 mm below the suspension's surface. After the ultrasonic treatment, the starch suspension was filtered and dried in a cabinet dryer at 50 °C for 24 h. The dried starch was then ground and sieved through a 100-mesh sieve. To assess the impact of extraction factors on starch yield efficiency, 3 variables were considered: ultrasonic power (60 - 120 W), extraction time (10 - 30 min), and sample-to-solvent ratio (1:20 - 1:40) [23,29]. The starch yield was calculated using the following equation:

$$Starch\ yeild\ (\%) = \frac{w2}{w1} \times 100\ \% \quad (1)$$

W1 represents the sample weight, and w2 denotes the amount of starch released following the ultrasonic treatment.

Porang starch extraction from porang flour

Porang starch was extracted from porang flour prepared by slicing porang tubers into 3 mm slices, drying at 60 °C, and grinding into flour [27]. The flour was mixed with water in an appropriate ratio, stirred into a homogeneous suspension, and filtered through a fine satin cloth. The filtrate was spun in a centrifuge at 4,000 rpm for 15 min. The supernatant was carefully decanted without disturbing the starch sediment. The sediment was dried at 50 °C for 24 h, then ground and sifted to obtain PS [27,28].

Experimental design

A Box-Behnken Design (BBD) was utilized to optimize the extraction conditions, implemented using Design Expert 13 software (Stat-Ease, Inc., USA). The optimization focused on 3 process factors, each evaluated at 3 levels, as outlined in **Table 1**. The response variable for the BBD was the yield of starch extraction. The experimental design included 15 runs, featuring 3 replicated center points conducted in random order, as shown in **Table 2**.

Table 1 Optimization code levels for starch isolation from porang glucomannan extraction residue.

Variable	Code	−1	0	+1
Sonication power (W)	x_1	60	90	120
Time extraction (min)	x_2	10	20	30
Solid-solvent ratio (g/mL)	x_3	1:20	1:30	1:40

Table 2 RSM experimental design of extraction showing the actual and predicted starch yields.

Run order	Sonication power (W)	Time extraction (min)	Solid-solvent ratio (g/mL)	Yield (%)	
				Actual	Predicted
1	90	30	1:20	35.45	36.22
2	90	20	1:30	54.12	53.97
3	60	10	1:30	39.78	39.56
4	120	30	1:30	45.32	45.55
5	60	20	1:40	57.58	58.84
6	90	20	1:30	53.35	53.97
7	60	30	1:30	49.33	48.85
8	90	20	1:30	54.44	53.97
9	90	10	1:40	61.30	60.54
10	90	10	1:20	40.07	40.57
11	120	10	1:30	52.41	52.89
12	90	30	1:40	67.36	66.85

Run order	Sonication power (W)	Time extraction (min)	Solid-solvent ratio (g/mL)	Yield (%)	
				Actual	Predicted
13	60	20	1:20	47.12	46.84
14	120	20	1:40	76.88	77.16
15	120	20	1:20	39.55	38.56

In addition, a statistical analysis of variance (ANOVA) was performed on the quadratic models to assess their validity.

$$Y = A_0 + \sum_{i=1}^{3} A_i X_i + \sum_{i=1}^{3} A_{ii} X_i^2 + \sum_{i=1}^{2} \sum_{j=i+1}^{3} A_{ij} X_i X_j \quad (2)$$

In this equation, Y represents the response, A0 is a constant, Ai is the coefficients for the linear terms, Aii and Aij are the coefficients for the quadratic terms, and Xi and Xj denote the values of the factors being studied.

Characterization of starch

Chemical composition

The moisture content, starch content, amylose, and amylopectin of the prepared starch were measured following the AOAC method [30].

Color

A small amount of the finely ground starch sample was placed in a petri dish, and its color values were measured using a colorimeter (CR-400 Chroma meter set, Konica Minolta, Japan). The L, a, and b color values, which correspond to lightness (0 to 100), green-red (− to +), and blue-yellow (− to +) spectra, respectively, were recorded.

FT-IR Analysis

The functional groups of the samples were examined using a Fourier Transform Infrared (FTIR) spectrophotometer (Thermo Scientific Nicolet iS10, USA) within a wavelength range of 400 to 4,000 cm^{-1}. A small amount of KBr powder was added to each sample as a binder. After conducting infrared deconvolution (with a peak half-width of 19 cm^{-1} and a resolution enhancement factor of 1.9), the absorbance ratios at 1,047/1,022, 995/1,022, 927/1,080, and 1,500/1,080 cm^{-1} were calculated to evaluate the short-range ordered structure of the starch.

Scanning electron microscopy (SEM)

The morphological characteristics of the samples were investigated using scanning electron microscopy (SEM) (JSM-6510LA, JEOL Ltd, Japan). The samples were lightly spread over an aluminum stub and coated with a thin layer of platinum (0 mm thick) using an SEM coating unit before being examined under the microscope.

X-Ray diffractometer (XRD)

The crystallinity profiles of the samples were obtained using an X-ray diffractometer (XRD) (Bruker AXS D8 Advance (Eco), Germany), operating at a voltage of 40 kV and a current of 25 mA. It utilized a monochromatic Cu K “beta” radiation filter with a wavelength of 0.139225 nm, scanning at an angle of 2θ = 0 - 100 ° with a step size of 0.01 ° and a step time of 2 s.

Differential scanning calorimeter (DSC)

The transition temperature and enthalpy change of the starch samples during gelatinization were measured using a Differential Scanning Calorimeter (DSC) (Shimadzu DSC-60 Plus, Japan). Each sample, with a total dry matter content of approximately 2 mg, was heated from 30 to 300 °C at a rate of 10 °C per min.

Statistical analysis

The experimental data were analyzed using the least squares method in multiple regression analysis. Pareto analysis of variance (ANOVA) at a 95 % confidence level ($p < 0.05$) was performed to calculate the linear, quadratic, and interaction coefficients of the regression model, assessing the significance of process variables. The F-value predicted error sum of squares (PRESS), and predicted R^2 were used to evaluate the model’s adequacy. Response Surface Methodology (RSM) was employed using the Design Expert statistical

software version 13 (Stat Ease Inc., USA) to determine the optimal starch yield response.

Results and discussion

Response surface methodology approach

This study focused on optimizing the starch yield from PR by determining the ideal ultrasonic extraction parameters: Sonication power, extraction time, and solid-solvent ratio. These parameters were chosen based on the ranges provided in **Table 1**. Using a Box-Behnken Design (BBD), 15 experiments with different input combinations were carried out to identify the optimal conditions for the combined effects of the 3 process variables. The experimental design matrix and corresponding extraction results are detailed in **Table 2**. The collected data were analyzed using multiple regression to fit a second-order quadratic polynomial. The resulting model equation, expressed in coded process variables, is shown in Eq. (3). Term B was excluded from the equation as it had an insignificant effect on the overall process, as confirmed by the analysis of variance.

$$Yield(\%) = 53.97 + 2.51A + 12.65C - 4.16AB + 6.65\,AC + 2.67\,BC - 1.48A^2 - 5.78B^2 + 2.86C^2 \quad (3)$$

The experiment used a statistical model comprising linear, quadratic, and 2-factor interaction terms (2FI). Variables A, B, and C represented sonication power, extraction time, and solid-solvent ratio, respectively, alongside interaction (AB, AC, BC) and quadratic terms (A^2, B^2, C^2). The constant value of 53.97 indicated the baseline extraction yield with process variables set to zero. The solid-solvent ratio was the most influential factor ($p < 0.05$), increasing yield by 12.65 % per unit change.

ANOVA confirmed the model's significance ($p < 0.005$, F-value = 198.33). Variable B, with a high *p*-value (0.2252), was deemed insignificant and excluded from Eq. (3). The model showed high accuracy with R^2 = 0.9972, adjusted R^2 = 0.9922, and predicted R^2 = 0.9602, indicating a strong fit to the experimental data. The lack-of-fit test (p = 0.1833) showed no significant deviation, supporting model compatibility. The low CV (1.93 %) indicated high reproducibility, consistent with studies by Noor *et al.* [21] and Ali *et al.* [23]. The AP value of 50.2580, well above the threshold of 4, confirmed the model's precision and reliability [29].

Model adequacy

The regression model's effectiveness in predicting responses was evaluated through adequacy checks, including ANOVA to validate the polynomial regression model. Diagnostic residual analysis (**Figure 1**) revealed a strong linear correlation between predicted and experimental data, confirming a solid relationship between process variables and starch yield. The normality of residuals was assessed using the standard probability plot, while the model's goodness-of-fit was evaluated with studentized residuals and average probability percentages. **Figure 1(B)** further illustrates the consistency between predicted and actual yields. Additionally, the adjusted R-squared (AdjR^2) value in **Table 3** shows that the model explains 99.2 % of the variation in extraction yield, with both interaction and individual factor effects considered. An AdjR^2 above 70 % and R^2 greater than 0.9 indicate model validation adequacy [22,25].

Table 3 Analysis of variance for the regression coefficients of the fitted polynomial quadratic model on starch yield.

Source	Sum of squares	df	Mean square	F-value	*p*-value
Model	1,777.09	9	197.45	198.33	< 0.0001
A-Sonication Power	50.38	1	50.38	50.60	0.0009
B-Time extraction	1.90	1	1.90	1.91	0.2252
C-solid: Solvent ratio	1,280.32	1	1,280.32	1,286.01	< 0.0001
AB	69.18	1	69.18	69.48	0.0004
AC	176.95	1	176.95	177.73	< 0.0001

Source	Sum of squares	df	Mean square	F-value	*p*-value
BC	28.43	1	28.43	28.56	0.0031
A^2	8.06	1	8.06	8.10	0.0360
B^2	123.44	1	123.44	123.99	0.0001
C^2	30.13	1	30.13	30.26	0.0027
Residual	4.98	5	0.9956		
Lack of Fit	4.35	3	1.45	4.61	0.1833
Pure Error	0.6285	2	0.3142		
Cor Total	1,782.07	14			
Std. Dev.	0.9978			R^2	0.9972
Mean	51.62			Adj R^2	0.9922
C.V. %	1.93			Pred R^2	0.9602
RESS	71.01			Adeq Precision	50.2579

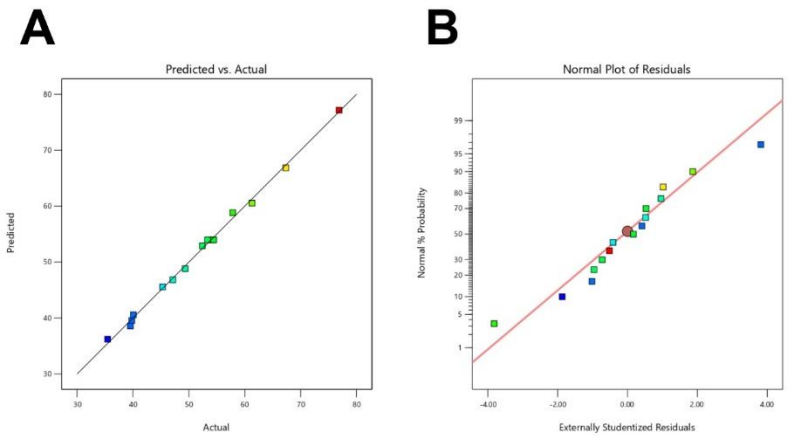

Figure 1 (A) The diagnostic plots of internally studentized residuals against average % probability and (B) the predicted extraction yield compared to the actual extraction yield.

Effect of process variables

This study optimized 3 process variables—sonication power, extraction time, and solid-solvent ratio—through a Box-Behnken Design (BBD) response surface methodology. The model generated 3-dimensional (3D) response surfaces and 2-dimensional (2D) contour plots, as depicted in **Figure 2**. The 3D plots aid in understanding by holding 2 factors constant to highlight the interactive effects on the variables. The dependent variable in these interactions was used to determine the optimal condition [19,22,26].

Effect of sonication power

The impact of varying sonication power (60 - 120 W) on starch yield was explored. As sonication power increased, starch yield rose, with the highest yield observed at 120 W when paired with an optimal solid-to-solvent ratio (**Figure 2(B)**), indicating a synergistic effect between these parameters. The optimal sonication power for maximum starch yield was found to be 119.97 W. This result aligns with previous research, which indicates that higher sonication power intensifies acoustic cavitation effects, aids in the breakdown of cellular matrices, and speeds up the release of cell contents [15]. Moreover, increased sonication power has

been reported to generate greater turbulence, which improves solvent penetration into the sample matrix [31].

Effect of time extraction

Sonication time is a critical variable significantly affecting starch extraction from PR. **Figure 2** shows that starch yield gradually increased with sonication time, peaking at 18.89 min. Beyond this point, the yield declined, particularly at lower solid-solvent ratios (**Figure 2(C)**). This finding aligns with previous studies that reported sonication time as a crucial factor in providing sufficient duration for cavitation processes to operate effectively [21,25]. After reaching the optimal point, the decrease in starch yield can be attributed to the breakdown of the starch structure due to extended exposure to ultrasonic mechanical forces and heat [18].

Effect of solid-solvent ratio

The solid-solvent (SS) ratio is another important factor affecting starch yield. This study evaluated different SS ratios between 1:20 and 1:40 g/mL, showing a significant effect on starch yield. With the optimal settings for the other 2 process variables (sonication power of 119.97 W and extraction time of 18.89 min), a solid-solvent ratio of 1:39.88 g/mL was found to be ideal for maximizing starch yield. Higher solid-solvent ratios increase the availability of solvent relative to the sample, enhancing solvent penetration into plant tissues and improving the dissolution and diffusion of active components, including starch [19,22]. Conversely, lower ratios limit contact between the sample and solvent, reducing extraction efficiency. This finding aligns with other research indicating that a larger solvent ratio enhances solvent diffusion into the tissue matrix. While higher ratios improve diffusion, excessively high values dilute the starch concentration in the solvent, potentially complicating downstream separation and increasing process costs [31].

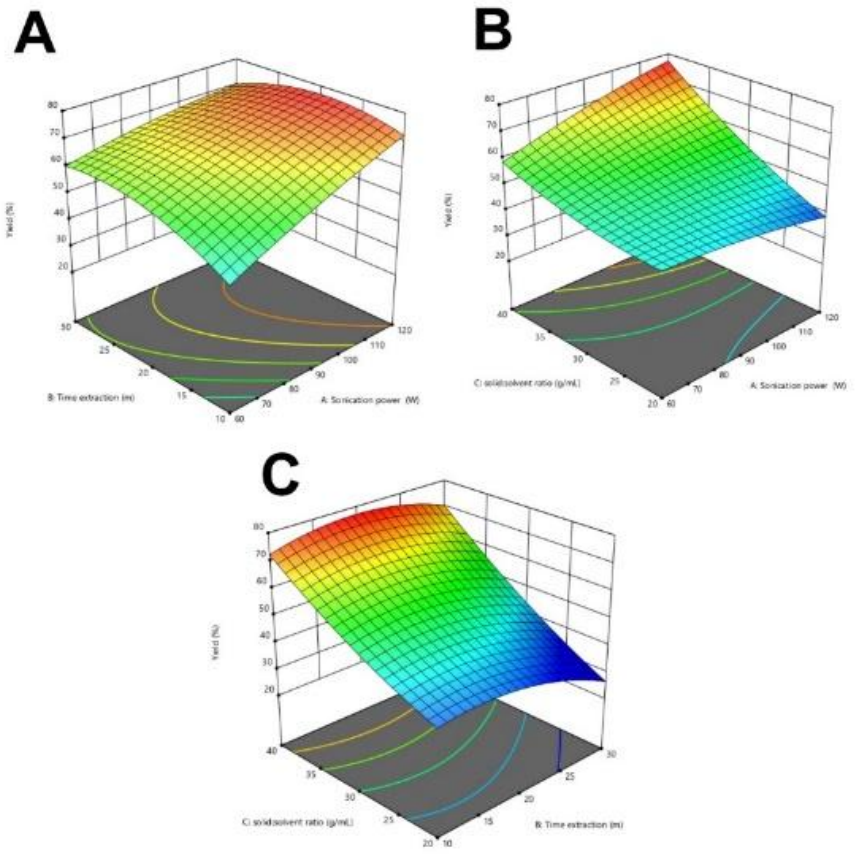

Figure 2 3D response surface and 2D plots illustrating starch yield as a result of the interaction between (A) sonication power and extraction time, (B) sonication power and solid-solvent ratio, and (C) extraction time and solid-solvent ratio.

Verification of predictive model

A multivariate regression model (Eq. (3)) was applied to optimize the extraction process for achieving the highest yield from fresh cassava tubers. The optimal conditions determined were a sonication power of 119.97 W, an extraction time of 18.89 min, and a solid-solvent ratio of 39.88 g/mL. With these parameters, the predicted starch yield was 76.90 %, targeting a value of 1.0. Three confirmation experiments were conducted to validate the optimized conditions, yielding an average starch yield of 77.54 ± 0.99 %, which surpassed the predicted value of 76.90 %. The experimental results aligned with the optimized model, yielding higher starch recovery than the 75.98 % reported by Noor *et al.* [21] for sago pith waste. This demonstrates the effectiveness of RSM in optimizing variables and enhancing extraction efficiency. The model's robustness offers potential for industrial scaling and broader application to other plant-based residues, with future studies needed to evaluate its scalability and feasibility.

Characterization of starch

Chemical composition

Based on the chemical composition presented in **Table 4**, OPS had the highest moisture content (9.46 %), while PF had the lowest (7.68 %), with OPRS exhibiting a similar moisture level to PF. Starch content was also highest in OPS (67.80 %) and lowest in OPRS (55.69 %), indicating superior starch extraction efficiency in OPS. Additionally, amylose content was significantly higher in OPS (24.73 %) compared to other samples, whereas OPRS had the lowest amylose content (7.51 %). Conversely, amylopectin content was highest in OPRS (48.18 %) and lowest in OPS (43.07 %). These results highlight differences in chemical composition across the samples, influenced by the source material and extraction methods, with OPS demonstrating the highest starch and amylose content, suggesting superior extraction efficiency and potential functionality.

Table 4 Chemical composition of porang flour (PF), porang starch (PS) optimized porang starch (OPS), and optimized porang glucomannan extraction residue starch (OPRS).

Parameter	Samples			
	PF	PS	OPS	OPRS
Moisture (%)	7.68 ± 0.38^{a}	8.40 ± 0.41^{ab}	9.46 ± 1.28^{b}	7.72 ± 0.98^{a}
Starch (%)	59.71 ± 0.15^{b}	60.97 ± 0.16^{c}	67.80 ± 0.29^{d}	55.69 ± 0.38^{a}
Amylose (%)	13.95 ± 0.04^{c}	13.63 ± 0.05^{b}	24.73 ± 0.10^{d}	7.51 ± 0.07^{a}
Amylopectin (%)	45.76 ± 0.16^{b}	47.35 ± 0.12^{c}	43.07 ± 0.20^{a}	48.18 ± 0.35^{d}

Each value is expressed as the mean ± Standard Deviation (n=5). Values with distinct letters are significantly different ($p < 0.05$) according to one-way ANOVA with DMRT post-hoc test.

These findings align with or contrast previous studies on porang-based materials. For instance, Suriati *et al.* [32] reported that the moisture content of porang flour ranged from 19.39 to 24.85 %, while Anggela *et al.* [33] noted a lower moisture content of 12.29 %. Nurman *et al*. [1] observed that porang starch had a moisture content of 13.39 – 15.89 %, with starch content between 41.63 and 63.30 %, and amylopectin levels ranging from 28.58 to 42.85 %. The comparatively lower moisture content in OPS and OPRS in this study indicates a closer alignment with processed starch or flour products, while the higher starch and amylose content in OPS underscores the effectiveness of the extraction method employed.

Color

Based on the color parameters in **Table 5** and **Figure 4**, the L* value (lightness) was highest in OPRS (65.12) and OPS (65.63), indicating they are the lightest samples, whereas PF had the lowest L* value (58.32). The* value (red-green axis) was significantly higher in OPS (11.05), showing a reddish tone, while OPRS had the lowest a* value (2.25), indicating a greener hue. The b* value (yellow-blue axis) was lowest in OPS (4.76)

and highest in PF (12.45), suggesting PF has a more pronounced yellow tone.

The whiteness index was highest in OPRS (63.89) and OPS (63.64), indicating more excellent visual whiteness compared to PF (56.19) and PS (58.34). This demonstrates the effectiveness of RSM in optimizing variables and enhancing extraction efficiency. The model's robustness offers potential for industrial scaling and broader application to other plant-based residues, with future studies needed to evaluate its scalability and feasibility [32,34]. The color parameters observed in this study align with Herawati *et al*. [35], who reported similar trends in porang flour. Compared to conventional methods, the optimized UAE approach produces starch with superior lightness and whiteness, making it ideal for food and cosmetic applications where visual quality is critical.

Table 5 Colour of porang flour (PF), porang starch (PS) optimized porang starch (OPS), and optimized porang glucomannan extraction residue starch (OPRS).

Parameter	Samples			
	PF	PS	OPS	OPRS
L*	58.32 ± 0.01^{a}	59.98 ± 0.01^{b}	65.63 ± 0.01^{d}	65.12 ± 0.01^{c}
a*	5.23 ± 0.02^{c}	4.76 ± 0.03^{b}	11.05 ± 0.01^{d}	2.25 ± 0.01^{a}
b*	12.45 ± 0.02^{d}	10.55 ± 0.01^{c}	4.31 ± 0.04^{a}	9.07 ± 0.01^{b}
Whiteness index	56.19 ± 0.01^{a}	58.34 ± 0.01^{b}	63.64 ± 0.01^{c}	63.89 ± 0.01^{c}

Each value is expressed as the mean ± Standard Deviation (n=5). Values with distinct letters are significantly different ($p < 0.05$) according to one-way ANOVA with DMRT post-hoc test.

FTIR spectra analysis

Figure 3(A) shows peaks around 3,400 cm^{-1} (O-H stretching) [36]. Peaks at 2,920 - 2,930 cm^{-1} (C-H stretching) and 1,640 cm^{-1} (C=O stretching or bound water) are typical of polysaccharides in starch granules [37,38]. Peaks between 1,000 - 1,200 cm^{-1} (C-O and C-C stretching) confirm the starch's structural integrity, with sharper peaks in OPS and OPRS reflecting the UAE method's success in enhancing purity. Key peaks at 1,160, 1,080, and 930 cm^{-1} correspond to C-O vibrations, confirming the presence of polysaccharides, while peaks at 1,650 and 1,350 cm^{-1} indicate C=O and C–O–C bonds, characteristic of starch granules [39,40]. These results align with Azhar *et al.* [8] and Sarifudin *et al*. [41], who observed similar FTIR spectra, further supporting the study's structural and compositional findings.

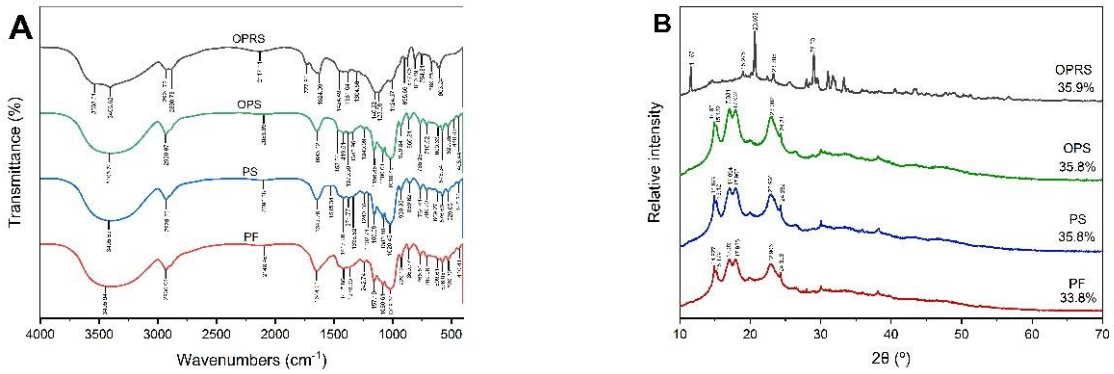

Figure 3: (a) FTIR spectra and (b) XRD patterns of Porang Flour (PF), Porang Starch (PS), Optimized Porang starch (OPS), and Optimized Porang Glucomannan Extraction residue Starch (OPRS).

XRD

Native starch from plant tissues is generally classified into A, B, or C types based on differences in crystallinity. Based on **Figure 3(b)**, the diffractograms display distinct peaks at various 2θ values, indicative of the sample's crystalline nature. The crystallinity index is highest for OPRS (35.9 %), followed closely by OPS and PS (both at 35.8 %), while PF exhibits the lowest crystallinity at 33.8 %. The presence of characteristic peaks around 14.9, 17.9, 22.9, and 24.3 ° suggests that these samples maintain typical starch crystalline structures, such as the A-type or C-type polymorphs [42-44]. However, OPRS exhibits additional, more intense peaks, likely due to residual glucomannan or other compounds introduced during the extraction process, which could enhance crystallinity through secondary structural interactions [35]. These results indicate that the optimized extraction process (OPS) maintains starch crystallinity while enhancing yield, with the slightly higher crystallinity in OPRS reflecting its waste-derived origin. The optimized extraction process (OPS) preserves starch crystallinity while improving yield, with the slightly higher crystallinity in OPRS reflecting its waste-derived origin. Starches with higher crystallinity offer benefits such as improved thermal stability, as their tightly packed crystalline regions resist degradation at higher temperatures [45]. This makes high-crystallinity starch ideal for bioplastic production, providing structural integrity and serving as a sustainable alternative to starch-base bioplastic [24]. Overall, these findings demonstrate that the optimized extraction method (OPS) preserves starch crystallinity while enhancing purity and yield, whereas OPRS, derived from waste, exhibits slightly higher crystallinity due to residual structural components, highlighting the impact of source material on starch properties.

Scanning electron microscopy

Based on **Figure 4**, PF exhibits a coarse texture and light brown color, reflecting its less processed state. The granules of PF are irregular, dominated by round and oval shapes, with an average particle size ranging from 6.5 to 20 μm, indicating a heterogeneous size distribution, resembling potato starch and sweet potato starch [20,43]. In contrast, PS and OPS appear finer and whiter, indicating higher purity, while OPRS, though fine, retains some coloration due to its derivation from waste materials. Microscopic analysis at ×1,000 magnification reveals that PF has irregular particle shapes, typical of raw flour [41]. PS and OPS show more uniform, spherical granules, with OPS exhibits slightly more homogeneous and intact granules, likely due to the optimized extraction conditions reducing mechanical stress and preventing excessive fragmentation during processing. The particle size of PS ranges from 7.64 - 20 μm, and OPS has an average particle size of 6.98 - 13.68 μm. OPRS, however, displays irregular and broken granules, likely due to structural degradation during glucomannan extraction [27], with particle sizes ranging from 7.62 to 24 μm. At ×5,000 magnification, PF shows rough surfaces with visible impurities, while PS and OPS display smooth, spherical granules characteristic of high-purity starch, similar to ultrasound-treated corn and cassava starch [46]. OPRS displays fragmented and rough granules, likely caused by the mechanical and thermal stresses during glucomannan extraction, which disrupts the granule structure and increases surface irregularities [33,47].

Overall, the findings demonstrate that OPS achieves better granule uniformity and smoothness than PS, validating the effectiveness of the optimization process. Meanwhile, OPRS, derived from extraction residue, retains some starch properties but exhibits compromised granule integrity due to extraction stresses [48]. These results highlight the potential for enhancing porang-based products through optimization and utilizing waste materials in value-added applications.

Differential scanning calorimetry

Table 6 shows that PF has the lowest enthalpy (−162.47 J/g), indicating lower starch content and refinement. PS has the highest enthalpy (−209.87 J/g), reflecting greater crystallinity and purity. OPS has slightly lower enthalpy (−198.25 J/g), suggesting structural changes from optimization, while OPRS has moderate enthalpy (−170.23 J/g), influenced by its waste-derived origin and extraction process. In terms of gelatinization, PF has the highest Tf (150.50 °C) and widest range (6.77 °C), indicating heterogeneity, while PS has the lowest to (133.58 °C) and Tf (140.55 °C), reflecting high purity. OPS shows higher temperatures (To: 156.98 °C, Tf: 162.43 °C), indicating optimization

effects. OPRS has the highest Tf (164.05 °C) and a narrower gelatinization range (4.90 °C), indicating improved thermal stability, which may enhance its suitability for applications requiring higher thermal resistance, such as in food processing or bioplastic production. OPS and OPRS exhibit narrower gelatinization ranges (5.45 and 4.90°C), implying more uniform and stable crystalline structures. Thermodynamic analysis confirms gelatinization as a melting process of starch crystallization [48]. In Nurman *et al* [1], porang starch from Pandeglang had To, Tp, and ΔHg values of 83.08, 88.71 °C, and 8.04 J/g, respectively. The lower enthalpy in these samples suggests weaker crystalline structures, likely due to lower purity or processing effects increasing the amorphous structure.

Table 6 DSC properties of porang flour (PF), porang starch (PS) optimized porang starch (OPS), and optimized porang glucomannan extraction residue starch (OPRS).

Samples	ΔH (J g^{-1})	To (°C)	Tp (°C)	Tf - To (°C)	Tf(°C)
PF	−162.47	143.73	145.81	6.77	150.50
PS	−209.87	133.58	135.79	6.97	140.55
OPS	−198.25	156.98	158.73	5.45	162.43
OPRS	−170.23	159.15	160.82	4.90	164.05

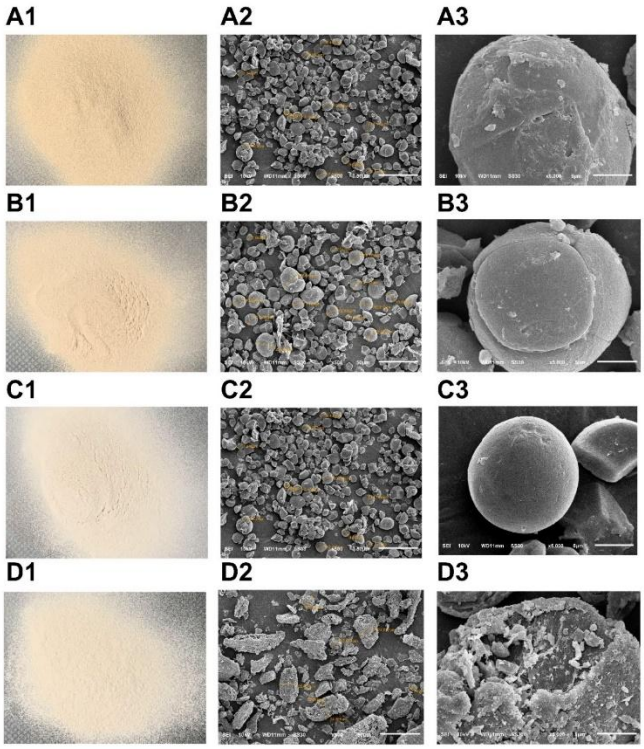

Figure 4: Images of PF (A), PS (B), OPS (C), and OPRS (D) with Scanning electron micrograph at ×500 magnification (2) ×5,000 magnification (3).

Conclusions

This study optimized starch extraction from PR using an RSM-Box-Behnken design with 3 factors: Sonication power, extraction time, and solid-solvent ratio. The model, with an R^2 of 0.9972, confirmed its suitability for the experimental data. Optimal conditions were 119.97 W sonication power, a 1:39.88 g/mL solid-solvent ratio, and 18.89 min extraction time, The

experimental yield of 77.54 %, which surpassed the predicted value of 76.90 %, confirming UAE's effectiveness for industrial starch extraction. Optimized porang starch (OPS) had the highest starch (67.80 %) and amylose (24.73 %) content, while starch from extraction residue (OPRS) showed lower starch (55.69 %) and amylose (7.51 %) but higher amylopectin (48.18 %). Color analysis indicated effective pigment removal and FTIR spectra confirmed the purity and structural integrity of OPS and OPRS. XRD analysis revealed OPS crystallinity, while DSC showed improved thermal stability and enhanced gelatinization properties in OPS and OPRS, highlighting their potential for applications in food, bioplastics, and pharmaceutical industries due to their enhanced purity, structural integrity, and thermal stability.

Acknowledgments

The author would like to thank the supervisors of this research from the Faculty of Agricultural Technology, Gadjah Mada University.

References

[1] N Nurman, M Silahudin, N Muda and TR Maulani. Karakterisasi fisikokimia pati porang pandeglang banten. *Gorontalo Agriculture Technology Journal* 2022; **5(2)**, 55-62.

[2] A Maghfirah, S Sudiati, SNKB Sitepu and M Widyanti. The effect of using a combination of sorbitol and glycerol plasticizers on the characterization of edible film from porang (amorphophallus oncophyllus) starch. *Journal of Technomaterials Physics* 2023; **5(2)**, 86-92.

[3] AC Kumoro, DS Retnowati and R Ratnawati. Chemical compositions changes during hot extrusion at various barrel temperatures for porang (*amorphophallus oncophyllus*) tuber flour refining. *Journal of Physics Conference Series* 2019; **1175**, 012279.

[4] SB Widjanarko, E Widyastuti and FI Rozaq. Pengaruh lama penggilingan tepung porang (amorphophallus muelleri blume) dengan metode ball mill (cyclone separator) terhadap sifat fisik dan kimia tepung porang. *Jurnal Pangan Dan Agroindustri* 2015; **3(3)**, 867-877.

[5] A Yanuriati, DW Marseno, Rochmadi and E Harmayani. Characteristics of glucomannan isolated from fresh tuber of Porang (Amorphophallus muelleri Blume). *Carbohydrate Polymers* 2017; **156**, 56-63.

[6] R Satiti, T Utami, J Widada and E Harmayani. Characterization and prebiotic activity *in vitro* of hydrolyzed glucomannan extracted from fresh porang tuber (amorphophallus oncophyllus). *Trends in Sciences* 2024; **22(1)**, 8617.

[7] A Asben, D Syukri, NNT Nguyen and F Kasim. Application of flour extracted from porang (amorphophallus muelleri blume) in formulating peel-off mask. *Asian Journal of Plant Sciences* 2024; **23(3)**, 377-385.

[8] B Azhar, S Gunawan, ERF Setyadi, L Majidah, F Taufany, L Atmaja and HW Aparamarta. Purification and separation of glucomannan from porang tuber flour (*Amorphophallus muelleri*) using microwave assisted extraction as an innovative gelatine substituent. *Heliyon* 2023; **9(11)**, e21972.

[9] AIW Harimawan. Glucomannan from porang (Amorphophallus muelleri) improves short-chain fatty acid in wistar rat with high-fat and high-fructose diet. *Babali Nursing Research* 2024; **5(2)**, 297-307.

[10] N Tahar, D Wahyuni, R Adawiyah, Khaerani and M Wahyuddin. Formulation and antibacterial activity of porang (amorphophallus muelleri blume) extract gel against propionibacterium acne. *Ad-Dawaa Journal of Pharmaceutical Sciences* 2023; **6(1)**, 83-92.

[11] JE Witoyo, E Ni'maturohmah and PAR Utoro. Recent trends in porang research via bibliometrics analysis approach. *Jurnal Ilmiah Universitas Batanghari Jambi* 2023; **23(3)**, 2723-2729.

[12] M Nasrullah, Purwoko and TC Sunarti. Acidic and enzymatic hydrolysis of glucomannan agroindustrial waste. *IOP Conference Series: Earth and Environmental Science* 2020; **472(1)**, 012006.

[13] AP Bonto, RN Tiozon, N Sreenivasulu and DH Camacho. Impact of ultrasonic treatment on rice starch and grain functional properties: A review. *Ultrasonics Sonochemistry* 2021; **71**, 105383.

[14] S Bouhallel, B Belhadi, R Souilah, D Djabali and B Nadjemi. Isolation of starch from seven pearl millet grain landraces by two processes; wet

milling and ultrasound application. *Algerian Journal of Enviromental Science and Technology* 2021; **7(1)**, 1687-1697.

[15] L Mieles-Gomez, SE Quintana and LA Garcia-Zapateiro. Ultrasound-assisted extraction of mango (mangifera indica) kernel starch: chemical, techno-functional, and pasting properties. *Gels* 2023; **9(2)**, 136.

[16] EM Satmalawati, Y Pranoto, DW Marseno and Y Marsono. The physicochemical characteristics of cassava starch modified by ultrasonication. *IOP Conference Series: Materials Science and Engineering* 2020; **980(1)**, 012030.

[17] SX Tan, A Andriyana, S Lim, HC Ong, YL Pang and GC Ngoh. Rapid ultrasound-assisted starch extraction from sago pith waste (SPW) for the fabrication of sustainable bioplastic film. *Polymers* 2021; **13(24)**, 4398.

[18] B Wang, Z Zhong, Y Wang, S Yuan, Y Jiang, Z Li, Y Li, Z Yan, l Meng and L Qiu. Recent progress of starch modification assisted by ultrasonic wave. *Food Science and Technology* 2023; **43**, e107522.

[19] S Ochoa and JF Osorio-Tobon. Isolation and characterization of starch from the purple yam (dioscorea alata) anthocyanin extraction residue obtained by ultrasound-assisted extraction. *Waste and Biomass Valorization* 2024; **15(1)**, 379-389.

[20] S Ochoa, MM Durango-Zuleta and JF Osorio-Tobon. Integrated process for obtaining anthocyanins rich-extract by ultrasound-assisted extraction and starch recovery from purple yam (Dioscorea alata): A techno-economic evaluation. *Biomass Conversion and Biorefinery* 2023; **13(12)**, 10605-10614.

[21] MHM Noor, N Ngadi, AN Suhaidi, IM Inuwa and LA Opotu. Response surface optimization of ultrasound-assisted extraction of sago starch from sago pith waste. *Starch - Stärke* 2022; **74(1-2)**, 2100012.

[22] N Nurlela, N Ariesta, E Santosa and T Mulandri. Physicochemical properties of glucomannan isolated from fresh tubers of Amorphophallus muelleri Blume by a multilevel extraction method. *Food Research* 2022; **6(4)**, 345-353.

[23] NSA Ali, K Muda, MZM Najib, MFM Amin, S Ismail, MFM Shahimin and FA Dahalan. Ultrasound-assisted extraction of starch from oil palm Trunk: An optimization by response surface methodology. *ASEAN Engineering Journal* 2023; **13(4)**, 19-27.

[24] MT Hossain, MA Shahid, S Akter, J Ferdous, K Afroz, KRI Refat, O Faruk, MSI Jamal, MN Uddin and MAB Samad. Cellulose and starch-based bioplastics: A review of advances and challenges for sustainability. *Polymer-Plastics Technology and Materials* 2024; **63(10)**, 1329-1349.

[25] W Setyaningsih, Karmila, RN Fathimah and MN Cahyanto. Process optimization for ultrasound-assisted starch production from cassava (manihot esculenta crantz) using response surface methodology. *Agronomy* 2021; **11(1)**, 117.

[26] P Vithu, SK Dash, K Rayaguru, MK Panda and M Nedunchezhiyan. Optimization of starch isolation process for sweet potato and characterization of the prepared starch. *Journal of Food Measurement and Characterization* 2020; **14**, 1520-1532.

[27] TD Handayani, E Harmayani and Y Pranoto. Karakteristik glukomanan tepung porang (amorphophallus oncophyllus) dengan berbagai metode ekstraksi kimia. *Jurnal Sains dan Teknologi Pangan* 2023; **8(3)**, 6360-6369.

[28] S Devereux, PS Shuttleworth, DJ Macquarrie and F Paradisi. Isolation and characterization of recovered starch from industrial wastewater. *Journal of Polymers and the Environment* 2011; **19(4)**, 971-979.

[29] RN Fathimah, AFA. Ishlahi, MN Cahyanto and W Setyaningsih. Ultrasound-assisted production of corn starch: Process design and optimization. *IOP Conference Series: Earth and Environmental Science* 2021; **712(1)**, 012014.

[30] AOAC International. *Official methods of analysis of the association of analytical chemist; association of official analytical chemists*. AOAC International, Virginia, 2005.

[31] AG Kia, A Ganjloo and M Bimakr. A short extraction time of polysaccharides from fenugreek (trigonella foencem graecum) seed using continuous ultrasound acoustic cavitation: Process optimization, characterization and biological activities. *Food and Bioprocess Technology* 2018; **11(12)**, 2204-2216.

[32] L Suriati, I Mangku, AM Chindrawati, NS Daamayanti, NS Kesumayasa and IW Putra. Analysis of the characteristics of porang flour as a coating material after treatment of nacl solution: Analysis of konjac flour after treatment of NaCl solution. *Sustainable Environment Agricultural Science* 2023; **7(2)**, 145-152.

[33] A Anggela, YS Nabila, R Ananda and EP Nainggolan. Comparison of chemical characteristics in chips and porang flour typical East Kalimantan with commercial porang flour as a functional food. *Jurnal Agrotek Ummat* 2023; **10(4)**, 351.

[34] E Julianti, Z Lubis, E Yusraini and Ridwansyah. Physicochemical characteristics of fiber rich flour from solid waste of purple sweet potato starch processing. *IOP Conference Series: Earth and Environmental Science* 2021; **924(1)**, 012038.

[35] H Herawati, S Zahratunnisa, E Kamsiati, D Anggraini, I Kurniasari, F Kusnandar, Suparlan, I Agustinisari, Sunarmani, M Bachtiar, T Zubaidi, Misgiyarta and S Suhirman. The effect of dry extraction process technology on characteristics of porang flour. *E3S Web of Conferences* 2023, **425**, 01001.

[36] NF Iskandar, LBC Cahyono, E Harmayani and LD Witasari. High purity glucomannan after ultrasonic-assisted extraction and α-amylaseliquefaction of porang (Amorphophallus oncophyllus) flour. *Food Research* 2024; **8(3)**, 242-251.

[37] R Lassoued, M Abderrabba, J Mejri, WN Benahmed, A Benhmed and M Ferhi. Physicochemical, morphological and functional characteristics of starch isolated from Quercus ilex and Quercus coccifera. *Emirates Journal of Food and Agriculture* 2023; **35(12)**, 1-8.

[38] GF Mohsin, WJ Al-Kaabi and AK Alzubaidi. Describing polymers synthesized from reducing sugars and ammonia employing FTIR spectroscopy. *Baghdad Science Journal* 2022; **19(6)**, 1297.

[39] X Chen, W Yao, F Gao, D Zheng, Q Wang, J Cao, H Tan and Y Zhang. Physicochemical properties comparative analysis of corn starch and cassava starch, and comparative analysis as adhesive. *Journal of Renewable Materials* 2021; **9(5)**, 979-992.

[40] E Sholichah, B Purwono, A Murdiati, A Syoufian and A Sarifudin. Extraction of glucomannan from porang (Amorphophallus muelleri Blume) with freeze-thaw cycles pre-treatment. *Food Sciences and Technology* 2023; **43**, e1423.

[41] A Sarifudin, L Ratnawati, N Indrianti, R Ekafitri, E Sholichah, N Afifah, D Desnilasari, P Nugroho and AD Yuniar. Evaluation of some analytical methods for determination of calcium oxalate in Amorphophallus muelleri flour. *Food Sciences and Technology* 2022; **42**, e09522.

[42] K Li, T Zhang, W Zhao, H Ren, S Hong, Y Ge and H Corke. Characterization of starch extracted from seeds of Cycas revoluta. *Frontiers in Nutrition* 2023; **10**, 1159554.

[43] D Yonata, P Triwitono, L Arsanti Lestari and Y Pranoto. Physicochemical and structural properties of resistant starch prepared from tacca tuber starch using autoclaving-cooling and acid hydrolysis treatments. *Trends in Sciences* 2024; **22(1),** 8822.

[44] AO Oladebeye, AA Oladebeye and JO Arawande. Physicochemical properties of wild yam (dioscorea villosa) starch. *International Journal of Food Science* 2023; **2023(1)**, 8868218.

[45] L Shi, K Guo, X Xu, L Lin, X Bian and Wei. Physicochemical properties of starches from sweet potato root tubers grown in natural high and low temperature soils. *Food Chemistry: X* 2024; **22**, 101346.

[46] A Rahaman, A Kumari, X Zeng, MA Farooq, R Siddique, I Khalifa, A Siddeeg, M Ali and MF Manzoor. Ultrasound based modification and structural-functional analysis of corn and cassava starch. *Ultrasonics Sonochemistry* 2021; **80**, 105795.

[47] I Chakraborty, S Pallen, Y Shetty, N Roy and N Mazumder. Advanced microscopy techniques for revealing molecular structure of starch granules. *Biophysical Reviews* 2020, **12(1)**, 105-122.

[48] X Huang, H Liu, Y Ma, S Mai and C Li. Effects of extrusion on starch molecular degradation, order–disorder structural transition and digestibility: A review. *Foods* 2022; **11(16)**, 2538.